

Self-Reinforced Thermoplastic Polyurethane Wrinkled Foams with High Energy Absorption Realized by Gas Cooling assisted Supercritical CO₂ Foaming

Jiashun Hu^a, Ruixing Gu^a, Hao-Yang Mi^{a,b}, Xin Jing^b, Maxwell Fordjour Antwi-Afari^c,
Binbin Dong^{a*}, Chuntai Liu^a, Changyu Shen^a*

^a National Engineering Research Center for Advanced Polymer Processing Technology, The Key Laboratory of Advanced Materials Processing & Mold of Ministry of Education, Zhengzhou University, Zhengzhou 450001, China

^b Key Laboratory of Advanced Packaging Materials and Technology of Hunan Province, Hunan University of Technology, Zhuzhou, 412007, China

^c College of Engineering and Physical Sciences, Aston University, Birmingham, B4 7ET, United Kingdom

Corresponding Authors:

H.Y. Mi E-mail: mihaoyang@zzu.edu.cn

B. Dong E-mail: dongbinbin@zzu.edu.cn

Declaration of Competing Interest:

The authors declare no competing financial interest.

Abstract:

Self-reinforcement of polymer foams by cellular structure manipulation is a cost-effective approach to boost their performance and extend their applicable fields. Herein, thermoplastic polyurethane (TPU) foams with special wrinkly structures were fabricated via a gas cooling assisted scCO₂ foaming process which employed a CO₂ flow to rapidly reduce the temperature of the foam and trigger the release of intramolecular stress in the form of macroscopic distortion via the formation of wrinkles on the cell surface. The wrinkly structure could be regulated by the key processing parameters, including foaming temperature (T), foaming pressure (P), waiting time (Δt), and temperature drop (ΔT), in the range of 1.61 μm to 2.16 μm . The wrinkled foams demonstrated superior compressive properties, recoverability, and energy absorption in cyclic compression tests compared with conventional foams with the same cell size. The wrinkled foam with a wrinkle wavelength of 1.77 μm achieved 153.0%, 2.83%, and 99.0% improvement in compressive modulus, recovery rate, and energy absorption, respectively. It also displayed a low energy loss coefficient of 3.50% which was only 31.48% of the conventional foam. This work provides a feasible approach to realize the self-reinforcement of TPU foams by creating wrinkly structures on the cell surface, and extends potential applications of wrinkled TPU foams in cushion and buffering.

Keywords: Thermoplastic polyurethane; Supercritical CO₂ foaming; Wrinkly structure; Gas cooling; Compressive property

1. Introduction

Polymer foams are increasingly used in various fields of our daily life, such as aerospace, transportation, automobile, building & construction, and medical due to their virtues of relatively low cost, lightweight, excellent flexibility, toughness, and impact tolerance, thermal/electrical/acoustic insulation properties, and so on.¹⁻⁹ Since the supercritical carbon dioxide (scCO₂) foaming technology was first proposed by Nuh,^{10,11} it has been recognized as a promising technique to produce thermoplastic polymer foams on a large scale due to its unique advantages of being efficient, economic, and eco-friendly.¹² Thermoplastic polyurethane (TPU) is an elastomer with excellent elasticity, abrasion resistance, aging resistance, biocompatibility, and low-temperature flexibility.¹³ TPU foams are widely used in applications including sound absorption, thermal insulation, cushioning, sports, etc.^{14,15} Producing TPU foams via scCO₂ foaming is becoming a more and more important approach since it avoids the use of chemical blowing agents that are potentially toxic to human beings.¹⁶ Developing TPU foams with superior performance, especially compressive and energy absorption properties, is beneficial for extending their potential applicable fields.

Manipulating the cellular structure of the foam and introducing nanofillers in the polymer matrix are typical means to enhance the mechanical properties of polymer foams. Nanofillers such as nano-clay,¹⁷ silica,^{18,19} carbon nanotubes,²⁰ and graphene²¹⁻²³ have been combined with TPU to develop TPU nanocomposite foams with enhanced cell density and mechanical properties. However, additional processing techniques like melt extrusion, compounding, and solution mixing are required to develop the nanocomposites in the first place, which inevitably increases both the material cost and the processing cost. Self-reinforcement of polymer foams by manipulating the microstructure is usually a more desired approach to fabricate polymer foams with enhanced mechanical properties. For example, Hu et al. fabricated microcellular TPU using

two-step batch foaming of 3D printed TPU preform with honeycomb structure, and realized 2.0-6.5 times improvement in compressive modulus and 3.6-6.4 times improvement in energy absorption.²⁴ Liao et al. developed a TPU foam with an oriented cell structure by incorporating polyimide gas barrier films in the scCO₂ foaming process. The compressive modulus and strength of the developed TPU foam increased by as much as 355% and 121%, respectively.²⁵ Wang et al. fabricated TPU foams with tunable cell structures and mechanical properties, and found that foams fabricated by the cooling ramp foaming had superior resilience and strength than the foams prepared via heating ramp foaming due to smaller size cell and higher cell density.²⁶

Other approaches have been developed to alter the cellular morphologies of polymer foams although mechanical properties were not investigated. For instance, a two-step depressurization approach has been used to fabricate low-density bi-modal foams containing large and small cells simultaneously.²⁷⁻²⁹ Wang et al. developed a stretching-assisted foaming process that introduced an extension strain on the sample during foaming and led to the formation of TPU foams with elongated cellular structures.³⁰⁻³² We recently fabricated skinless porous TPU films with sub-micro cell size on the film surface via a surface-constrained foaming process, and demonstrated their applications in energy harvesting.³³ Although various methods have been developed to manipulate the cell structure including cell size, cell density, and cell orientation, there are seldom strategies to adjust the morphology on the cell surface.

Wrinkling phenomena are ubiquitous in nature with dimensions (like periodicity and amplitude) spanning across multiple length scales, which endow the biological surfaces with unique and intriguing physical and chemical properties.³⁴⁻³⁷ Polymeric materials with wrinkled surfaces are generally fabricated on bilayer film-substrate systems with mismatch modulus by applying external stimuli (e.g. stretching and releasing or thermal treatment) to trigger surface instability.^{38,39} Wrinkled polymers have shown promising potentials in various fields including

medical treatment,⁴⁰⁻⁴² energy acquire & absorption,^{43,44} flexible electronics & wearable devices,⁴⁵⁻⁴⁷ and electromagnetic shielding.⁴⁸ However, most researches focused on the development of wrinkled films, the fabrication of wrinkled foams is fairly difficult since it requires precise internal stress control in 3D. We have recently developed a dynamic scCO₂ foaming approach that is capable to generate intramolecular stress by the scCO₂ flow field and trigger the formation of wrinkles on the cell surface during the subsequent foaming process.⁴⁹ The wrinkled foams exhibited superior compressive and energy absorption properties.⁵⁰ Nevertheless, the process would consume a significant amount of CO₂, which is cost-inefficient.

In the core-shell sphere system, inflation and deflation regulate the pressure difference inside and outside of the sphere. A theoretical study showed that the pressure difference would result in compressive stress on the sphere system and induce the formation of wrinkles on shells.^{51,52} Following this principle, Stoop et al. depressurized the inner pressure of a polydimethylsiloxane (PDMS)-coated elastomer hemisphere and successfully triggered the formation of wrinkles on the surface of the PDMS hemisphere.⁵³ In the scCO₂ foaming process, each cell could be regarded as a core-shell sphere system and the inner pressure would undergo a declining trend as the expansion of cells. If one can manipulate the pressure difference inside and outside of the cells, it could be possible to realize the formation of wrinkles on numerous cell surfaces at the same time.

In this study, we developed a gas cooling assisted scCO₂ foaming method which used a cold CO₂ flush to rapidly reduce the temperatures of the foams and the CO₂ gas inside of the cells. The pressure decrease inside of the cells led to the rapid release of intramolecular stress generated by the cell expansion in the form of macroscopic distortion, which resulted in the formation of micro-sized wrinkles on the cell surface. This process is highly time and cost-effective, and it had a minor effect on the morphology of cell size and cell density. The influence of the key

processing parameters, including foaming temperature (T), foaming pressure (P), waiting time (Δt), and temperature drop (ΔT), on the cell sizes and wrinkly structures were investigated in detail. The underlying mechanism, as well as the controlling principle of the wrinkly structure, were discussed specifically. In addition, the compressive and energy absorbing properties of the foams were studied comprehensively. The wrinkled foams with small wrinkle size possess excellent self-reinforcement properties with enhanced compressive modulus, strength, recoverability, and energy absorption.

2. Experimental Methods

2.1 Materials

TPU pellets with a density of 1.12 g/cm^3 and a Shore hardness of 87A were purchased from Aohua Plastics Co., Ltd, China. The CO_2 with a purity of 99.9% was supplied by Zhengzhou Yumeng Gas Co., Ltd, China.

2.2 Fabrication of wrinkled TPU foam

Figure 1 illustrates the process of scCO_2 foaming with gas cooling to prepare TPU foams with wrinkly structure. Briefly, pre-dried TPU pellets were placed in a vacuum-assisted hot compression machine (Y002, Zhengzhou Craftsman Machinery Equipment Co., Ltd, China) and molded at $200 \text{ }^\circ\text{C}$ under a pressure of 4000kg for 12 minutes with a vacuum degree of -84kPa. The molded TPU samples with 3 mm were placed in a high-pressure vessel and flushed with CO_2 for 2 min to eliminate the air in the vessel. Then, the vessel was pressurized to the saturation pressure P using CO_2 , which was regulated by a Teledyne ISCO 260D high-pressure syringe pump. Subsequently, the vessel was preheated to the saturation temperature T . The pressure and temperature were maintained constant for 2 hours to saturate the TPU samples with scCO_2 . Then, the outlet valve was opened to depressurize the vessel to the atmospheric pressure followed by

waiting for a short time (Δt) and gas cooling using scCO₂ flow. In the gas cooling stage, the pressure of the syringe pump was set to 5 MPa while maintaining the outlet valve open, so that the foamed TPU samples could be cooled by the CO₂ gas. Ultimately, the foamed TPU samples were taken out from the vessel once the temperature dropped in it reached ΔT and naturally cooled to room temperature.

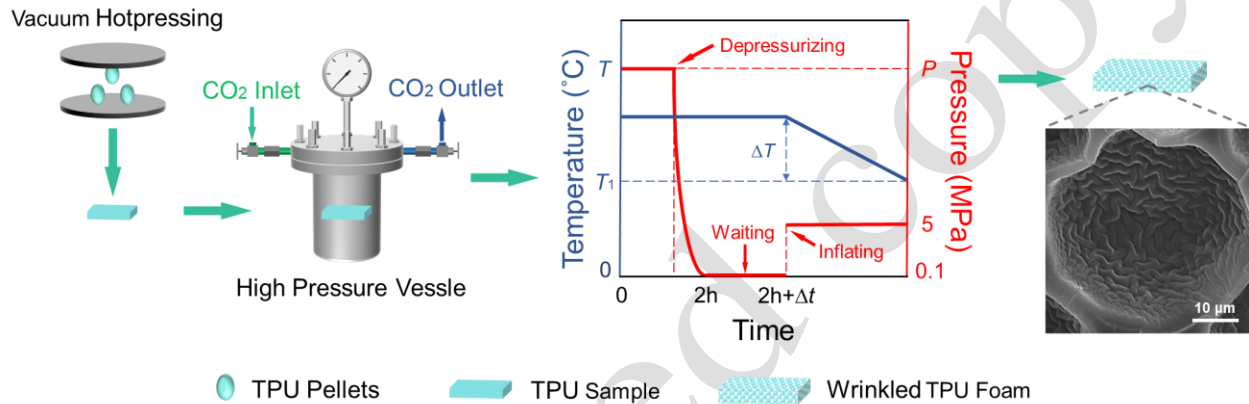


Figure 1. Schematic illustration of wrinkly TPU foams fabrication strategy.

The effects of critical factors in the gas cooling assisted scCO₂ foaming including foaming temperature (T), saturation pressure (P), waiting time (Δt), and temperature drop (ΔT) on the morphology of TPU foams were investigated by 9 trials of experiments listed in Table 1. TPU foams prepared under different conditions are labeled as T - P - Δt - ΔT . Trial 10 was conducted to investigate the effect of continuous gas-cooling on the formation of wrinkle structure. In the trial, TPU was foamed at 110 °C under 16 MPa, then the pressure was set to 5 MPa after depressurize while maintaining the outlet valve close for 1min followed by gas release and removing the foamed sample from the vessel.

Table 1. Nine trials of experiments with different parameters were carried out in this study.

	T (°C)	P (MPa)	Δt (s)	ΔT (°C)
1	100	16	0	10
2	110	16	0	10
3	120	16	0	10
4	110	12	0	10
5	110	20	0	10
6	110	16	15	10
7	110	16	30	10
8	110	16	0	0
9	110	16	0	20

2.3 Characterizations of foam structure

The thermal property of TPU was measured using a DSC apparatus (DSC Q2000, TA Instruments). TPU sample was heated from 30 °C to 180 °C and equilibrated for 3 min. Subsequently, it was cooled to -80 °C and then reheated to 180 °C. All heating and cooling cycles were conducted at a given rate of 5 °C/min. The morphologies of wrinkled TPU foams were investigated using field emission scanning electron microscopy (SEM, JEOL, Japan) at an acceleration voltage of 15 kV. The TPU foams were fractured using clamps after soaking in liquid nitrogen for 20 minutes, followed by coating a thin layer of gold on the fractured surface. The cell size, cell density, and wavelength of wrinkles were measured from SEM images using Image-Pro Plus software. More than 100 cells were measured to acquire the average cell size for each foam. The cell density was measured and calculated using the following equation:

$$N_f = \left(\frac{nM^2}{A} \right)^{3/2} \quad (1)$$

Where N_f (cm^{-3}) refers to the cell density of the samples, M is the magnification factor, n is the number of cells within a micrograph, whose area is A (cm^2).

The wavelength of the wrinkles (λ) formed on the surface was measured from the SEM images using Image-Pro Plus software. The wavelength was referred to the distance between the vertices of adjacent wrinkles (Figure S1),⁵⁴ and the measurements were performed on the wrinkles located at the bottom of the cells to minimize the effect of view error (Figure S2).

The density of TPU foams was measured using a scale, and the porosity of TPU foams were calculated using the following equation.

$$V_f = 1 - \frac{\rho_f}{\rho_s}$$

Where V_f refers to the porosity of TPU foam, ρ_f is the density of TPU foam, ρ_s is the density of solid TPU. For each TPU foam, the density measurement was conducted three times and the average value was calculated.

2.4 Characterization of compressive properties

The compressive properties of TPU foams were measured using a universal testing machine (UTM2203, Shenzhen Suns Technology Stock Co., Ltd, China). Cuboid TPU specimen with sizes of $4 \text{ mm} \times 4 \text{ mm} \times 4 \text{ mm}$ was used for cyclic compressive tests. At least 5 specimens was measured for each group. Cyclic compressive tests were performed by compressing the samples to 50% strain and released to 0% strain for 100 cycles at a cross-head speed of 10 mm/min. The samples were also cyclically compressed to 80 % strain for 10 cycles at a cross-head speed of 10 mm/min to evaluate their response at a high strain. In addition, cyclic compressive tests with the constant stress of 0.2 MPa were performed on different foams at a cross-head speed of 10

mm/min for 10 cycles. The recovery rate was defined as the percentage of deformation recovered in a cycle relative to the total deformation in that cycle. For each TPU foam, the cyclic compressive test was conducted five times, and the most representative compressive curves were presented.

The instant resilience performance of different TPU foams was characterized by calculating their energy absorption and release values in each loading-releasing cycle. By integrating the compression curve of each cycle, the energy loss ΔU and the energy loss coefficient $\Delta U/U$ in the cyclic compression processes can be calculated. The calculation formulae of ΔU and $\Delta U/U$ are as follows:

$$\Delta U = A_{Loading} - A_{Unloading} \quad (2)$$

$$\Delta U / U = \frac{A_{Loading} - A_{Unloading}}{A_{Loading}} \times 100\% \quad (3)$$

Where, $A_{Loading}$ and $A_{Unloading}$ are the areas enclosed by the stress-strain curve of the loading and unloading process, respectively, the energy absorption and energy release during the cyclic compressive processes.

3. Results and Discussion

3.1 Cell morphology and wrinkly structure

TPU samples were uniformly foamed under all the nine trials of experiments, and all foams showed normal cell diameter distribution (Figure S3). Six groups of foamed samples showed obvious wrinkly structures on their cell surfaces, while the other three groups had conventional smooth cell surfaces. The wavelengths of the wrinkles formed on all wrinkled foams displayed normal distribution with sizes ranging from 1.61 μm to 2.16 μm (Figure S4). Figure 2a-c shows the cellular morphology and the wrinkly structure of TPU foams fabricated under different

temperatures. It is found that there is no wrinkle on the cell surface of TPU foams foamed at 100 °C, while wrinkles could be seen when the saturation temperatures were 110 °C and 120 °C. The average cell size (Figure 2d) was increased from 18.2 μm to 28.7 μm, and the cell density (Figure 2e) was decreased from 1.22×10^8 /cm³ to 5.39×10^8 /cm³ as the foaming temperature was increased from 100 °C to 120 °C, which was because of the melt strength reduction of TPU with the increase of temperature.⁵⁵ The average wavelength results indicated that the wavelength of wrinkle was increased from 1.77 μm to 2.15 μm when the foaming temperature was enhanced from 110 °C to 120 °C suggesting the great influence of temperature on the wrinkly structure.

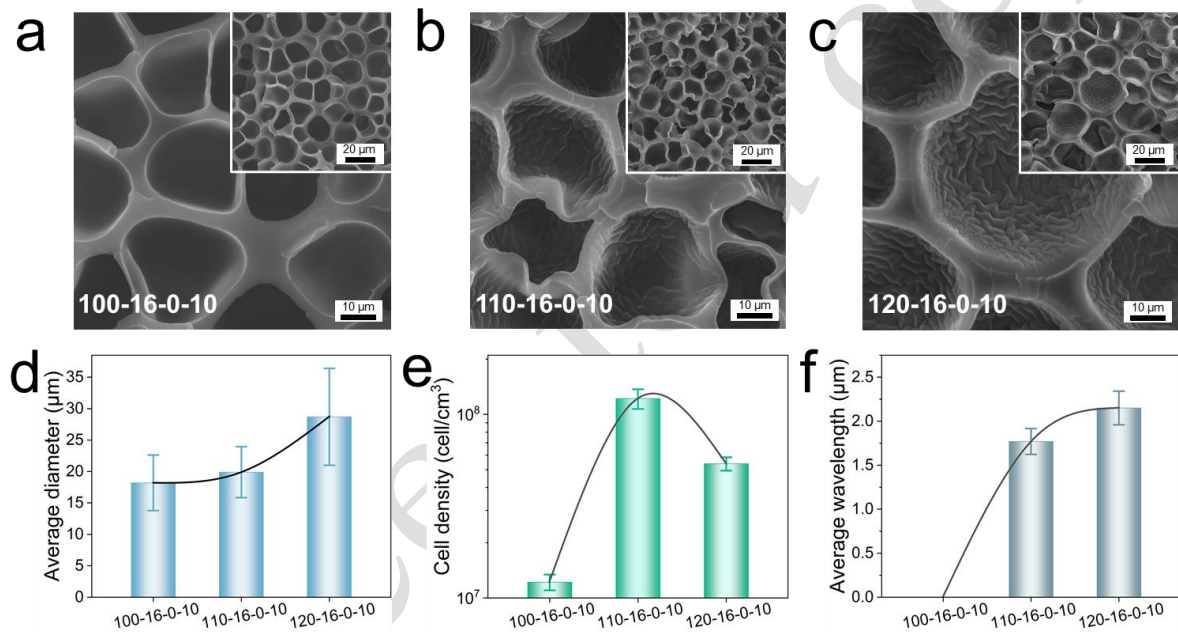


Figure 2. SEM images of TPU foams fabricated with different foaming temperatures (*T*): (a) 100-16-0-10 foam, (b) 110-16-0-10 foam, (c) 120-16-0-10 foam; (d) average cell diameter, (e) average cell density, and (f) average wavelength of wrinkles for different foams

Foaming pressure has significant effects on cellular morphology because it affects the cell nucleation in the foaming processes. Figure 3a-c shows the morphology of TPU foams prepared with different saturation pressure. It is clear that the cell size of the foams was decreased (Figure 3d) accompanied with a great increase of cell density (Figure 3e) as the foaming pressure was

increased from 12MPa to 20MPa since high cell nucleation rate under high pressure would cause the competing growth of cells and lead to smaller cell size.⁵⁶ In addition, it was found that no wrinkle was formed on the cell surface of the 110-12-0-10 foam, but dense wrinkles were observed when the saturation pressure was increased to 16 MPa and 20 MPa. As shown in Figure 3f, the wavelengths of wrinkles for the TPU foams prepared at 16 MPa and 20 MPa were 1.77 μm and 1.61 μm , respectively, which implies that the wrinkle size is negatively correlated with the foaming pressure.

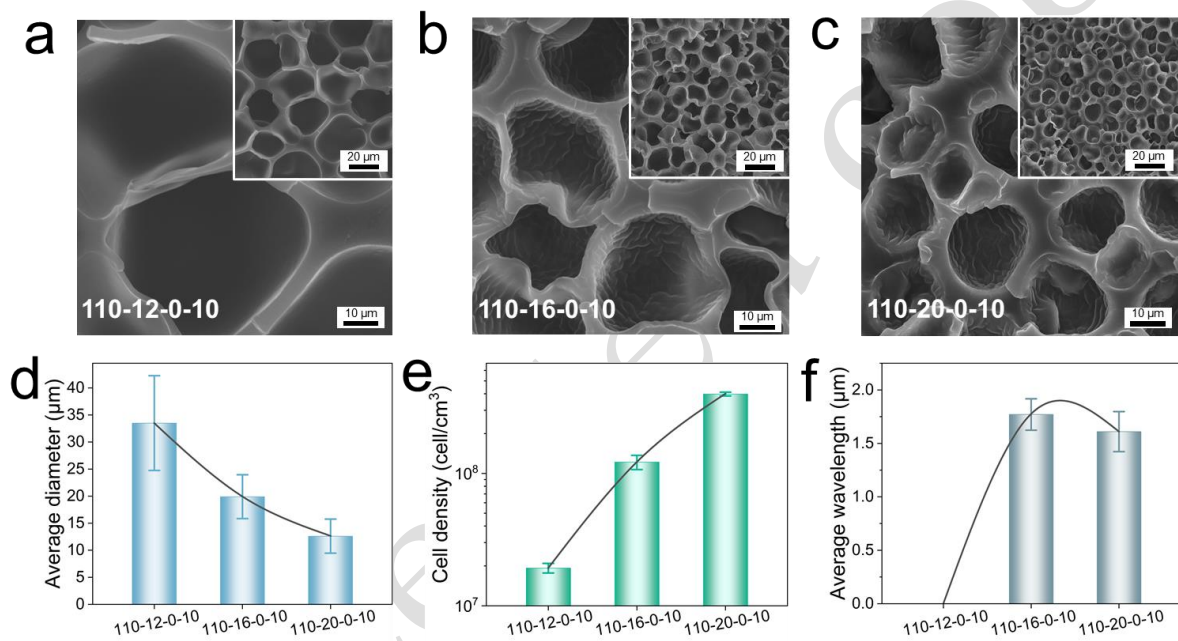


Figure 3. SEM images of TPU foams fabricated with different foaming pressure (P): (a) 110-12-0-10 foam, (b) 110-16-0-10 foam, (c) 110-20-0-10 foam; (d) average cell diameter, (e) average cell density, and (f) average wavelength of wrinkles for different foams

The waiting time (Δt) prior to the gas cooling is a governing factor that influences the growth time of cells before the gas cooling. The morphologies of TPU foams prepared with different Δt were shown in Figure 4a-c. It is seen that the difference in average cell size (Figure 4d) and cell density (Figure 4e) among various foams were insignificant as the increase of

waiting time from 0s to 30s. However, wrinkly structures were formed on all these foams, and the average wavelength was gradually increased from 1.77 μm to 2.16 μm as the increase of waiting time from 0s to 30s. It is clear that the wavelength of the wrinkles is positively correlated with the waiting time in the gas cooling assisted foaming process.

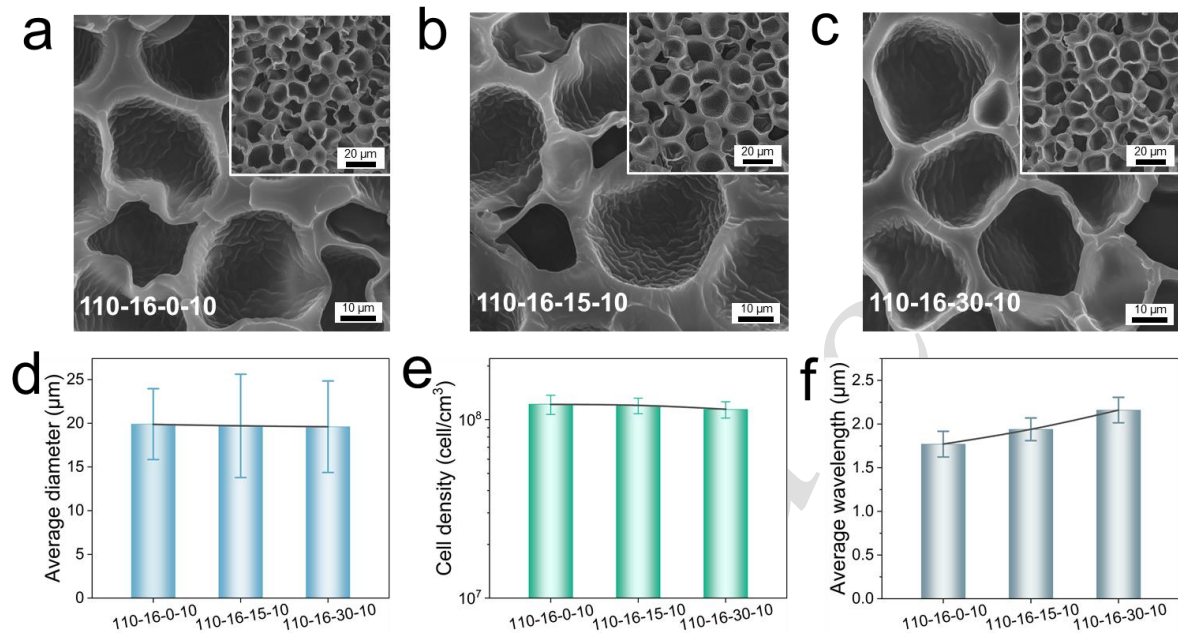


Figure 4. SEM images of TPU foams fabricated with different waiting time (Δt): (a) 110-16-0-10 foam, (b) 110-16-15-10 foam, (c) 110-16-30-10 foam; (d) average cell diameter, (e) average cell density, and (f) average wavelength of wrinkles for different foams

The temperature drop (ΔT) caused by the gas cooling is the key to generating the wrinkly structure on the cell surface. The ΔT of 0 $^{\circ}\text{C}$ indicates no gas cooling was applied, which is equivalent to the conventional scCO_2 foaming. It was found from Figure 5a-c that wrinkles are absent on the surface of the 110-16-0-0 foam, while dense wrinkles were presented on both 110-16-0-10 foam and 110-16-0-20 foam. The cell size of different foams was reduced from 19.8 μm to 17.9 μm as the ΔT was increased from 0 $^{\circ}\text{C}$ to 20 $^{\circ}\text{C}$ as shown in Figure 5d. The cell density of the foams showed an opposite trend (Figure 5e). As shown in Figure 5f, the wavelength of

wrinkles was reduced from 1.77 μm to 1.67 μm when the ΔT was increased from 10 $^{\circ}\text{C}$ to 20 $^{\circ}\text{C}$, which means that greater temperature drop is favorable for the formation of smaller and denser wrinkles. In addition, no wrinkly structure was formed on the cell surface of TPU foam fabricated under 5 MPa pressure without the gas-cooling process (Figure S5), which suggested that continuous gas-cooling is an important factor for the formation of wrinkly structures.

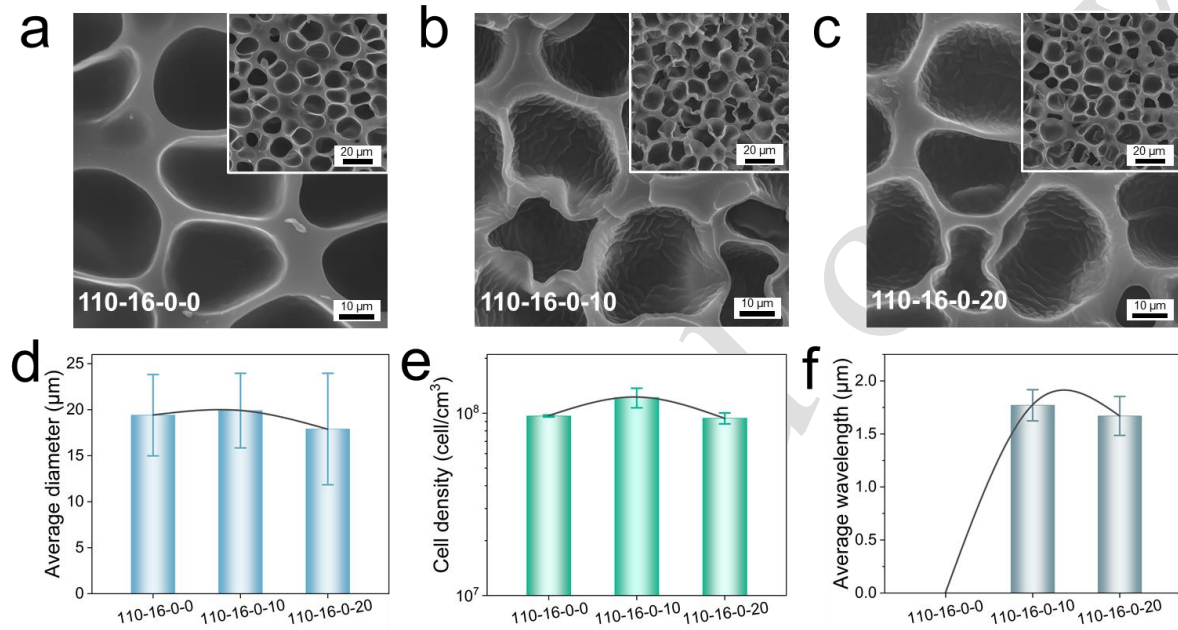


Figure 5. SEM images of TPU foams fabricated with different temperature drop (ΔT): (a) 110-16-0-0 foam, (b) 110-16-0-10 foam, (c) 110-16-0-20 foam; (d) average cell diameter, (e) average cell density, and (f) average wavelength of wrinkles for different foams

3.2 Formation mechanism and influencing factors of wrinkly structure

We have demonstrated that the gas cooling assisted scCO_2 foaming is capable to produce TPU foams with special wrinkly structures on the cell surface. Based on the morphology evolution as the change of processing conditions, we can deduce the mechanism for the formation of wrinkly structures on the cell surface in the gas cooling assisted scCO_2 foaming process. As illustrated in Figure 6a₁, the cell expansion that occurs in the foaming stage is triggered by the

internal high pressure of CO₂ gas (P_{CO_2}) and P_{CO_2} exceeds the surface tension of the TPU matrix ($\gamma_{Polymer-gas}$). As the growth of the cell, an equilibrium state would reach when the internal pressure is balanced by the surface tension.¹¹ Afterwards, the CO₂ in the cells will diffuse out from the foamed TPU gradually because of the pressure difference with the atmosphere during the solidification of TPU matrix. In conventional foaming, this process is quite slow so the intramolecular stress generated in TPU matrix during cell expansion could be gradually released, which normally causes uniform shrinking of cells and leads to the formation of smooth cell surfaces (Figure 6a₂). This is the case for the 110-16-0-0 foam which has uniform cellular morphology and a smooth cell surface.

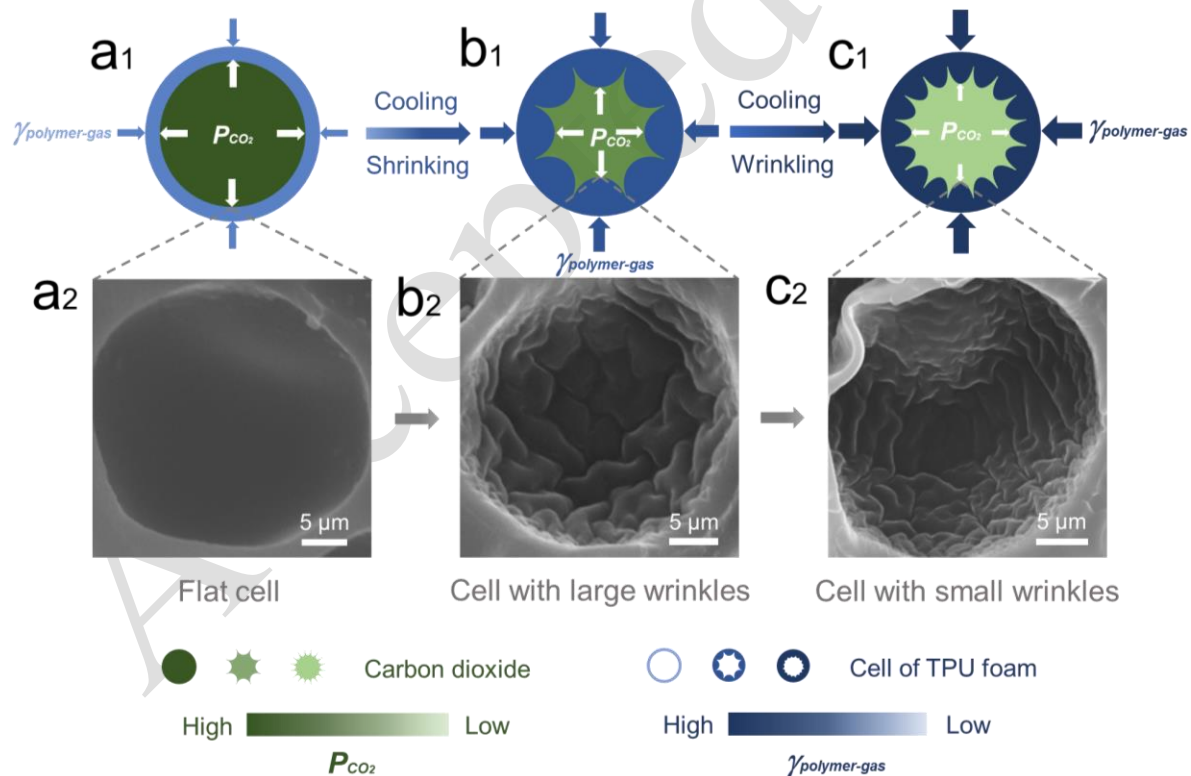


Figure 6. Schematic illustration of the formation mechanism of wrinkly structure in TPU foams.

(a₁) cell expansion in conventional foaming, (a₁) smooth cells formed in conventional foaming,

(b₁) small pressure difference with low ΔT , (b₂) large wrinkles formed in gas cooling assisted foaming with low ΔT , (c₁) large pressure difference with high ΔT , (c₂) dense wrinkles formed in gas cooling assisted foaming with high ΔT .

When the gas cooling was applied in the scCO₂ foaming, a rapid temperature drop (ΔT) would occur after or during the cell expansion depending on the waiting time (Δt). The temperature drop will cause the increase of $\gamma_{\text{Polymer-gas}}$ and the decrease of P_{CO_2} , which would accelerate the shrinkage of the cells as shown in Figure 6b₁. In this process, the intramolecular stress in the TPU cell surface could not release by molecular chain relaxation. Instead, the intramolecular stress tends to release in the form of macroscopic distortion via the formation of protuberous structures and wrinkles with large wavelengths (Figure 6b₂). When the ΔT was further increased, the macroscopic distortion on the cell surface would be more significant, so that a labyrinth-like wrinkly structure was formed on the cell surface as shown in Figure 6c.

In addition to the ΔT , it was found that T , P , and Δt had great influence on the formation of wrinkly structure. At a low foaming temperature (e.g. 100 °C), no wrinkles were formed since the TPU molecular chains were difficult to be stretched at a low temperature which led to insufficient intramolecular stress in the cell wall. The wrinkle wavelength for the foams prepared at T of 110 °C and 120 °C were 1.77 μm and 2.15 μm , respectively, with the same ΔT of 10 °C, which implies that the low $\gamma_{\text{Polymer-gas}}$ at high temperature is favorable for the formation of large wrinkles. The effect of foaming pressure (P) is significant on the structure of wrinkles. No wrinkles were formed at a low P of 12 MPa, and the wrinkle sizes for the foams prepared under 16 MPa and 20 MPa were 19.9 μm and 12.6 μm , respectively. The smaller wrinkle size at higher

P was caused by the high intramolecular stress generated by the fast expansion of cells under high P_{CO_2} , as well as the large P_{CO_2} reduction in the gas cooling stage.

Interestingly, the waiting time (Δt) had obvious influences on the wavelength of wrinkles but negligible effects on the cell size. With a long Δt (e.g. 30s), the intramolecular stress induced by cell expansion has more time to release by molecular chain relaxation rather than macroscopic distortion, which resulted in the formation of wrinkles with a large wavelength of 2.16 μm . However, the difference in cell size was negligible for the foams with different Δt . It is believed that the cell shrinkage is determined by the shrinkage during gas cooling and the shrinkage in nature cooling. For a highly elastic polymer like TPU, the shrinkage may take several days to fully complete. The shrinkage is basically caused by the combined effects of diffusion of CO_2 inside the cells and the release of intramolecular stress in TPU matrix. Therefore, extending Δt had limited influence on the final cell size while maintaining other conditions constant. In addition, DSC results indicated that the TPU had a tiny crystallization peak at 59 $^\circ\text{C}$ in the cooling process, and a small melting peak was detected at 154 $^\circ\text{C}$, which means that the TPU used was nearly amorphous. Thus, the pseudo-crosslinking structure formed by the hard segment would not play a significant role in the expansion and contraction process.

3.3 Compressive performance of the wrinkled foams

TPU foams with micro-sized closed cells have been extensively used in the application of cushion and buffering due to their excellent elasticity and energy absorption ability.⁵⁴⁻⁵⁷ To investigate the influence of wrinkly structure on the compressive property of TPU foams, cyclic compression tests were performed for up to 100 cycles on different TPU foams. In order to avoid the effect of cell size and cell density, wrinkled TPU foams prepared under different Δt were selected since their cell sizes were all about 19.6 μm . These wrinkled foams were denoted as WF1.77, WF1.94, and WF2.16 according to their wavelength. In addition, conventional foamed

TPU (110-16-0-0 foam) was chosen for comparison since its cell size (19.4 μm) is close to the wrinkled foams. The conventional foam was denoted as CF for simplicity. In addition, the cell density and porosity of CF, WF1.77, WF1.94, and WF2.16 are 0.221 g/cm^3 , 0.218 g/cm^3 , 0.220 g/cm^3 , 0.218 g/cm^3 , and 0.785, 0.788, 0.786, 0.788, respectively. Therefore, the cell diameter, cell density, foam density, and porosity of selected foams were close, which means that the difference in their mechanical property would mainly attributed to the wrinkly structure presented on cell surface.

Figure 7a shows the representative strain-stress curves of different TPU foams. It is clear that all foams had large hysteresis loss in the first cycle, then the cyclic compressive curves were gradually stabilized. The maximum compressive stress (σ_{max}) of four TPU foams at the 1st, 10th, 25th, 50th, and 100th cycles was compared in Figure 7b, from which it is obvious that the σ_{max} of the WFs was significantly higher than the CF, and the σ_{max} was higher for the WFs with smaller wrinkle wavelength. At the 100th cycle, the improvement in σ_{max} of WF1.77, WF1.94, and WF2.16 were 91.8%, 64.8%, and 40.3%, respectively, compared to the CF. The compressive moduli (E) calculated from the compression curves in each cycle of different foams were compared in Figure 7c. The E was reduced gradually as the increase of pressing cycles and the decrease became insignificant after the foams were pressed for 25 cycles. After compression for 100 cycles, the reduction in E were 16.1%, 9.3%, 10.9%, and 13.9% for CF, WF1.77, WF1.94, and WF2.16, respectively, which suggested that the WF with a small wrinkle size is more tolerant to cyclic compression. Comparing among different foams, the trend of E was the same with the σ_{max} results, and the WF1.77 showed a 153.0% improvement in E compared with the CF after 100 cycles of compression. These results further manifested the significant reinforcement effect of wrinkly structures on the TPU foams. Furthermore, the recovery rate results (Figure 7d) showed that the recovery rates of all foams were gradually increased and stabilized with the

increase of compression cycles because of the gradual stabilization of the unrecoverable damage and deformation in the foams. It was noticed that both the initial recovery rate and the recovery rate in the 100th cycle of wrinkled foams were much higher than the conventional foams, and the WF1.77 showed the highest recovery rate among all WFs suggesting that the presence of wrinkles on the cell surface would impede the bending of the cell wall and facilitate the recovery of the deformation.⁵⁸ In addition, the wrinkled foams with smaller wrinkle sizes exhibited higher energy absorption than the conventional foam as shown in Figure 7e, which was contributed by the stiffer cell wall and the high recoverability.

Furthermore, the cyclic compression property of the foams at high strain (e.g. 80%) was investigated. As shown in Figure 7f, the WF1.77 still had the highest compressive strength and recovery rate among all foams, and the wrinkled foams significantly outperformed the conventional foam. The energy absorption results (Figure 7g) demonstrated more obvious self-reinforcing effects of the wrinkly structure on the TPU foams. The energy absorption was increased by 147.0 % for the WF1.77 compared with the conventional foam. In addition, the cyclic compressive property of the foams with constant compressive stress was investigated for ten cycles. As shown in Figure 7h, the compressive strain of the CF was 50% under a compressive stress of 0.2 MPa, while the compressive strain of WF1.77, WF1.94, and WF2.16 were 27.9%, 33.9%, and 40.9%, respectively, which suggested low compressive deformation of the wrinkled foams. The energy loss coefficient results (Figure 7i) indicated that the energy loss relative to the energy absorption ($\Delta U/U$) of the WF1.77 was the lowest among all foams and the value in the 10th cycle was greatly lower than that of the 1st cycle. The $\Delta U/U$ of the WF1.77 was 3.50%, which was only 31.48% of the CF in the 10th cycle, which implies that the dense wrinkly structure is favorable for reducing energy loss and improving energy absorption while maintaining low energy loss.

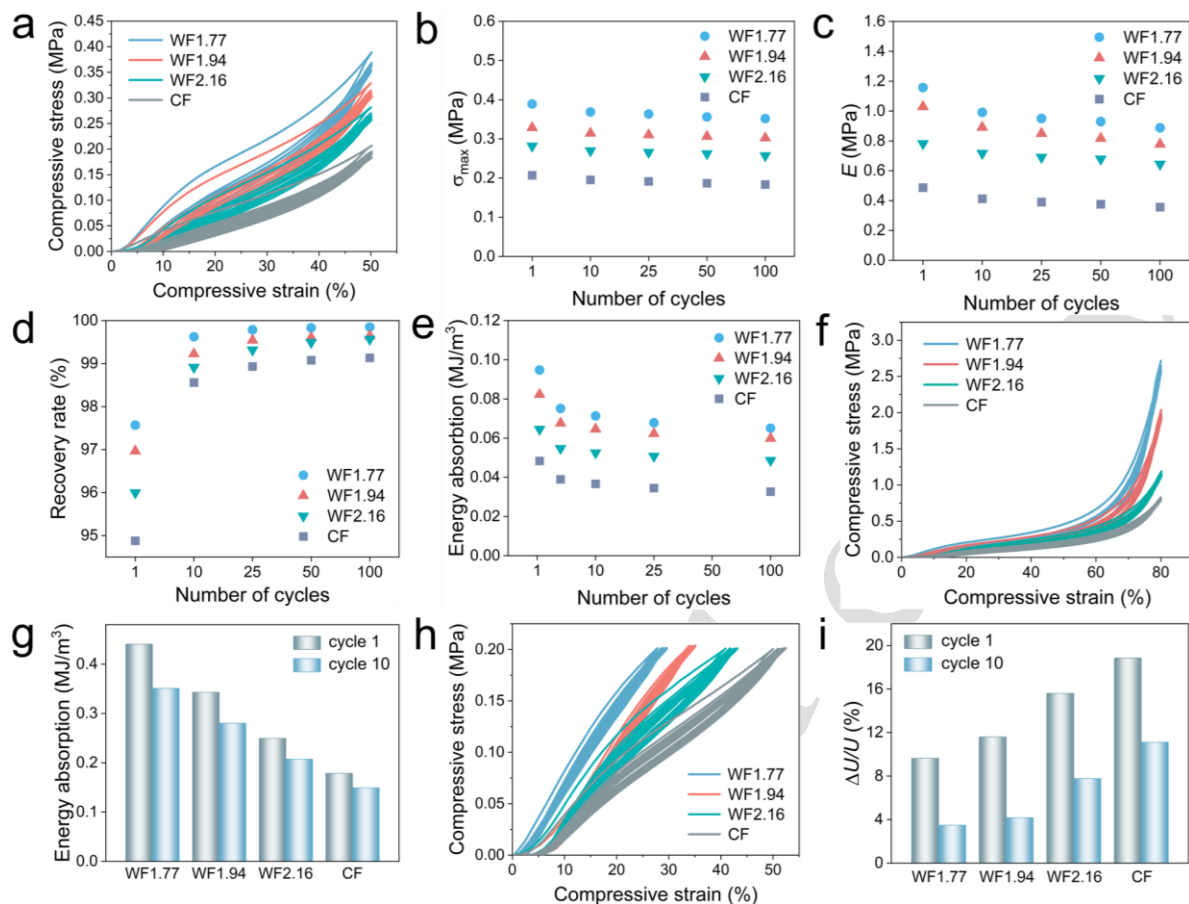


Figure 7. Cyclic compressive properties of wrinkled foams (WF) with different wrinkle wavelengths in comparison with the conventional foam (CF): (a) compressive stress-strain curves with a constant compressive strain of 50%, (b) compressive strength (σ_{max}) at 50% strain in different cycles, (c) compressive modulus (E) in different cycles, (d) recovery rate in different cycles, (e) energy absorption in different cycles, (f) compressive stress-strain curves with a constant compressive strain of 80%, (g) energy absorption in different cycles, (h) compressive stress-strain curves with a constant compressive stress of 0.2 MPa, and (i) energy loss coefficient ($\Delta U/U$) in different cycles.

4. Conclusion

In this study, TPU foams with special wrinkle structures were fabricated via a novel gas cooling assisted scCO₂ foaming process which introduced a period of CO₂ flow to rapidly reduce the temperature of the foamed TPU. The increase of matrix surface tension and the decrease of pressure inside the cells in the gas cooling process triggered the release of cell expansion intramolecular stress in the form of macroscopic distortion via the formation of wrinkles on the cell surface. The wrinkle structure was affected by the key processing parameters including foaming temperature (T), foaming pressure (P), waiting time (Δt), and temperature drop (ΔT). The wrinkle structure was not formed at a low temperature (e.g. 100 °C) or a low pressure (e.g. 12 MPa), or without the gas cooling step. Low T , high P , and large ΔT are favorable for reducing the wavelength of the wrinkles. Prolonging Δt will cause the increase of wrinkle wavelength, while it had negligible influence on the cell size and cell density. Compared with conventional foams, the wrinkled foams demonstrated superior compressive properties, recoverability, and energy absorption in cyclic compression tests. The foams with denser and smaller wrinkles exhibited remarkable self-reinforcement effects. The wrinkled foam with a wrinkle wavelength of 1.77 μm achieved 153.0%, 2.83%, and 99.0% improvements in the compression modulus, recovery rate, and energy absorption, respectively. It also possessed a low energy loss coefficient of 3.50% which was only 31.48% of the conventional foam.

Supporting Information

Illustration of the wrinkle wavelength; Wavelength measurement of wrinkle structures on cell surface; Cell diameter and wrinkle wavelength distribution of TPU foams fabricated with different foaming processes; DSC curves for TPU sample; SEM images of TPU foam fabricated in trial 10.

Acknowledgments

The authors are grateful for the financial support from the National Natural Science Foundation of China (52173049; 12072325), and the Natural Science Foundation of Hunan Province (2021JJ40177).

References

- (1) Hu, F.; Wu, S.; Sun, Y. Hollow-Structured Materials for Thermal Insulation. *Adv. Mater.* **2019**, *31* (38), e1801001. DOI: 10.1002/adma.201801001.
- (2) Zhao, S.; Malfait, W. J.; Guerrero-Alburquerque, N.; Koebel, M. M.; Nystrom, G. Biopolymer Aerogels and Foams: Chemistry, Properties, and Applications. *Angew. Chem., Int. Ed.* **2018**, *57* (26), 7580-7608. DOI: 10.1002/anie.201709014.
- (3) Wicklein, B.; Kocjan, A.; Salazar-Alvarez, G.; Carosio, F.; Camino, G.; Antonietti, M.; Bergstrom, L. Thermally insulating and fire-retardant lightweight anisotropic foams based on nanocellulose and graphene oxide. *Nat. Nanotechnol.* **2015**, *10* (3), 277-283. DOI: 10.1038/nnano.2014.248.
- (4) Forest, C.; Chaumont, P.; Cassagnau, P.; Swoboda, B.; Sonntag, P. Polymer nano-foams for insulating applications prepared from CO₂ foaming. *Prog. Polym. Sci.* **2015**, *41*, 122-145. DOI: 10.1016/j.progpolymsci.2014.07.001.
- (5) Alemán-Domínguez, M. E.; Ortega, Z.; Benítez, A. N.; Monzón, M.; Garzón, L. V.; Ajami, S.; Liu, C. Polycaprolactone–carboxymethyl cellulose composites for manufacturing porous scaffolds by material extrusion. *Bio-Des. Manuf.* **2018**, *1* (4), 245-253. DOI: 10.1007/s42242-018-0024-z.

- (6) Shao, L.; Gao, Q.; Xie, C.; Fu, J.; Xiang, M.; Liu, Z.; Xiang, L.; He, Y. Sacrificial microgel-laden bioink-enabled 3D bioprinting of mesoscale pore networks. *Bio-Des. Manuf.* **2020**, *3* (1), 30-39. DOI: 10.1007/s42242-020-00062-y.
- (7) Wang, Q.; Ma, Z.; Wang, Y.; Zhong, L.; Xie, W. Fabrication and characterization of 3D printed biocomposite scaffolds based on PCL and zirconia nanoparticles. *Bio-Des. Manuf.* **2020**, *4* (1), 60-71. DOI: 10.1007/s42242-020-00095-3.
- (8) Wang, G.; Zhao, J.; Wang, G.; Mark, L. H.; Park, C. B.; Zhao, G. Low-density and structure-tunable microcellular PMMA foams with improved thermal-insulation and compressive mechanical properties. *Eur. Polym. J.* **2017**, *95*, 382-393. DOI: 10.1016/j.eurpolymj.2017.08.025.
- (9) Wang, G.; Zhao, G.; Dong, G.; Mu, Y.; Park, C. B.; Wang, G. Lightweight, super-elastic, and thermal-sound insulation bio-based PEBA foams fabricated by high-pressure foam injection molding with mold-opening. *Eur. Polym. J.* **2018**, *103*, 68-79. DOI: 10.1016/j.eurpolymj.2018.04.002.
- (10) Martini-Vvedensky, J. E.; Suh, N. P.; Waldman, F. A. Microcellular closed cell foams and their method of manufacture. U.S. Patent 4,473,665, 1984.
- (11) Cha, S. W.; Suh, N. P.; Baldwin, D. F.; Park, C. B. Microcellular thermoplastic foamed with supercritical fluid. U.S. Patent 5,158,986, 1992.
- (12) Wang, W.; Liao, X.; He, Y.; Li, J.; Jiang, Q.; Li, G. Thermoplastic polyurethane/polytetrafluoroethylene composite foams with enhanced mechanical properties and anti-shrinkage capability fabricated with supercritical carbon dioxide. *The Journal of Supercritical Fluids* **2020**, *163*, 104861. DOI: 10.1016/j.supflu.2020.104861.

- (13) Ge, C.; Zhai, W. Cellular Thermoplastic Polyurethane Thin Film: Preparation, Elasticity, and Thermal Insulation Performance. *Ind. Eng. Chem. Res.* **2018**, *57* (13), 4688-4696. DOI: 10.1021/acs.iecr.7b05037.
- (14) Wu, B.; Wang, H.; Chen, Y.; Wang, Z.; Maertens, T.; Kuang, T.; Fan, P.; Chen, F.; Zhong, M.; Tan, J.; et al. Preparation and properties of thermoplastic polyurethane foams with bimodal structure based on TPU/PDMS blends. *J. Supercrit. Fluids* **2021**, *177*, 105324. DOI: 10.1016/j.supflu.2021.105324.
- (15) Qu, Z.; Yin, D.; Zhou, H.; Wang, X.; Zhao, S. Cellular morphology evolution in nanocellular poly (lactic acid)/thermoplastic polyurethane blending foams in the presence of supercritical N₂. *Eur. Polym. J.* **2019**, *116*, 291-301. DOI: 10.1016/j.eurpolymj.2019.03.046.
- (16) Ge, C.; Wang, S.; Zheng, W.; Zhai, W. Preparation of microcellular thermoplastic polyurethane (TPU) foam and its tensile property. *Polym. Eng. Sci.* **2018**, *58* (S1), E158-E166. DOI: 10.1002/pen.24813.
- (17) Wang, X. C.; Jing, X.; Peng, Y. Y.; Ma, Z. K.; Liu, C. T.; Turng, L. S.; Shen, C. Y. The effect of nanoclay on the crystallization behavior, microcellular structure, and mechanical properties of thermoplastic polyurethane nanocomposite foams. *Polym. Eng. Sci.* **2016**, *56* (3), 319-327. DOI: 10.1002/pen.24257.
- (18) Li, J.; Liao, X.; Han, W.; Xiao, W.; Ye, J.; Yang, Q.; Li, G.; Ran, Q. Microcellular nanocomposites based on millable polyurethane and nano-silica by two-step curing and solid-state supercritical CO₂ foaming: Preparation, high-pressure viscoelasticity and mechanical properties. *J. Supercrit. Fluids* **2017**, *130*, 198-209. DOI: 10.1016/j.supflu.2017.08.003.
- (19) Yang, J.; Huang, L.; Zhang, Y.; Chen, F.; Fan, P.; Zhong, M.; Yeh, S. A New Promising Nucleating Agent for Polymer Foaming: Applications of Ordered Mesoporous Silica

- Particles in Polymethyl Methacrylate Supercritical Carbon Dioxide Microcellular Foaming. *Ind. Eng. Chem. Res.* **2013**, 52 (39), 14169-14178.
- (20) Fei, Y.; Chen, F.; Fang, W.; Xu, L.; Ruan, S.; Liu, X.; Zhong, M.; Kuang, T. High-strength, flexible and cycling-stable piezo-resistive polymeric foams derived from thermoplastic polyurethane and multi-wall carbon nanotubes. *Composites, Part B* **2020**, 199, 108279. DOI: 10.1016/j.compositesb.2020.108279.
- (21) Liu, H.; Dong, M.; Huang, W.; Gao, J.; Dai, K.; Guo, J.; Zheng, G.; Liu, C.; Shen, C.; Guo, Z. Lightweight conductive graphene/thermoplastic polyurethane foams with ultrahigh compressibility for piezoresistive sensing. *J. Mater. Chem. C* **2017**, 5 (1), 73-83. DOI: 10.1039/c6tc03713e.
- (22) Shi, S.; Zhang, Y.; Luo, Y.; Liao, X.; Li, G. Reinforcement of Mechanical Properties of Silicone Rubber Foam by Functionalized Graphene Using Supercritical CO₂ Foaming Technology. *Ind. Eng. Chem. Res.* **2020**, 59 (51), 22132-22143.
- (23) Kuang, T. R.; Mi, H. Y.; Fu, D. J.; Jing, X.; Chen, B. Y.; Mou, W. J.; Peng, X. F. Fabrication of Poly(lactic acid)/Graphene Oxide Foams with Highly Oriented and Elongated Cell Structure via Unidirectional Foaming Using Supercritical Carbon Dioxide. *Ind. Eng. Chem. Res.* **2015**, 54 (2), 758–768.
- (24) Hu, B.; Li, M.; Jiang, J.; Zhai, W. Development of microcellular thermoplastic polyurethane honeycombs with tailored elasticity and energy absorption via CO₂ foaming. *Int. J. Mech. Sci.* **2021**, 197, 106324. DOI: 10.1016/j.ijmecsci.2021.106324.
- (25) Li, J.; Liao, X.; Jiang, Q.; Wang, W.; Li, G. Creating orientated cellular structure in thermoplastic polyurethane through strong interfacial shear interaction and supercritical carbon dioxide foaming for largely improving the foam compression performance. *J. Supercrit. Fluids* **2019**, 153, 104577. DOI: 10.1016/j.supflu.2019.104577.

- (26) Wang, G.; Wan, G.; Chai, J.; Li, B.; Zhao, G.; Mu, Y.; Park, C. B. Structure-tunable thermoplastic polyurethane foams fabricated by supercritical carbon dioxide foaming and their compressive mechanical properties. *J. Supercrit. Fluids* **2019**, *149*, 127-137. DOI: 10.1016/j.supflu.2019.04.004.
- (27) Li, C.; Feng, L. F.; Gu, X. P.; Cao, K.; Zhang, C. L. In situ visualization on formation mechanism of bi-modal foam via a two-step depressurization approach. *J. Supercrit. Fluids* **2018**, *135*, 8-16. DOI: 10.1016/j.supflu.2017.12.005.
- (28) Gong, P.; Wang, G.; Tran, M. P.; Buahom, P.; Zhai, S.; Li, G.; Park, C. B. Advanced bimodal polystyrene/multi-walled carbon nanotube nanocomposite foams for thermal insulation. *Carbon* **2017**, *120*, 1-10. DOI: 10.1016/j.carbon.2017.05.029.
- (29) Xu, L.; Qian, S.; Zheng, W.; Bai, Y.; Zhao, Y. Formation Mechanism and Tuning for Bimodal Open-Celled Structure of Cellulose Acetate Foams Prepared by Supercritical CO₂ Foaming and Poly(ethylene glycol) Leaching. *Ind. Eng. Chem. Res.* **2018**, *57* (46), 15690-15696.
- (30) Wang, G.; Zhao, J.; Yu, K.; Mark, L. H.; Wang, G.; Gong, P.; Park, C. B.; Zhao, G. Role of elastic strain energy in cell nucleation of polymer foaming and its application for fabricating sub-microcellular TPU microfilms. *Polymer* **2017**, *119*, 28-39. DOI: 10.1016/j.polymer.2017.05.016.
- (31) Zhao, J.; Wang, G.; Zhang, A.; Zhao, G.; Park, C. B. Nanocellular TPU composite foams achieved by stretch-assisted microcellular foaming with low-pressure gaseous CO₂ as blowing agent. *J. CO₂ Util.* **2021**, *53*, 101708. DOI: 10.1016/j.jcou.2021.101708.
- (32) Huang, P.; Wu, F.; Pang, Y.; Wu, M.; Lan, X.; Luo, H.; Shen, B.; Zheng, W. Enhanced dispersion, flame retardancy and mechanical properties of polypropylene/intumescent flame

- retardant composites via supercritical CO₂ foaming followed by defoaming. *Compos. Sci. Technol.* **2019**, *171*, 282-290. DOI: 10.1016/j.compscitech.2018.12.029.
- (33) Ni, G. L.; Zhu, X.; Mi, H. Y.; Feng, P. Y.; Li, J.; Jing, X.; Dong, B.; Liu, C.; Shen, C. Skinless porous films generated by supercritical CO₂ foaming for high-performance complementary shaped triboelectric nanogenerators and self-powered sensors. *Nano Energy* **2021**, *87*, 106148. DOI: 10.1016/j.nanoen.2021.106148.
- (34) Wang, Q.; Zhao, X. Beyond wrinkles: Multimodal surface instabilities for multifunctional patterning. *MRS Bull.* **2016**, *41* (2), 115-122. DOI: 10.1557/mrs.2015.338.
- (35) Tan, Y.; Hu, B.; Song, J.; Chu, Z.; Wu, W. Bioinspired Multiscale Wrinkling Patterns on Curved Substrates: An Overview. *Nano-Micro Lett.* **2020**, *12* (1), 101. DOI: 10.1007/s40820-020-00436-y.
- (36) Rodríguez-Hernández, J. Wrinkled interfaces: Taking advantage of surface instabilities to pattern polymer surfaces. *Prog. Polym. Sci.* **2015**, *42*, 1-41. DOI: 10.1016/j.progpolymsci.2014.07.008.
- (37) Mei, Y.; Kiravittaya, S.; Harazim, S.; Schmidt, O. G. Principles and applications of micro and nanoscale wrinkles. *Mater. Sci. Eng. R Rep.* **2010**, *70* (3-6), 209-224. DOI: 10.1016/j.mser.2010.06.009.
- (38) Zeng, S.; Li, R.; Freire, S. G.; Garbellotto, V. M. M.; Huang, E. Y.; Smith, A. T.; Hu, C.; Tait, W. R. T.; Bian, Z.; Zheng, G.; et al. Moisture-Responsive Wrinkling Surfaces with Tunable Dynamics. *Adv. Mater.* **2017**, *29* (24). DOI: 10.1002/adma.201700828.
- (39) Rhee, D.; Lee, W. K.; Odom, T. W. Crack-Free, Soft Wrinkles Enable Switchable Anisotropic Wetting. *Angew. Chem., Int. Ed.* **2017**, *56* (23), 6523-6527. DOI: 10.1002/anie.201701968.

- (40) Kim, J.; Yoon, J.; Hayward, R. C. Dynamic display of biomolecular patterns through an elastic creasing instability of stimuli-responsive hydrogels. *Nat. Mater.* **2010**, *9* (2), 159-164. DOI: 10.1038/nmat2606.
- (41) Gan, Y.; Jiang, X.; Yin, J. Self-Wrinkling Patterned Surface of Photocuring Coating Induced by the Fluorinated POSS Containing Thiol Groups (F-POSS-SH) as the Reactive Nanoadditive. *Macromolecules* **2012**, *45* (18), 7520-7526. DOI: 10.1021/ma301439g.
- (42) Kim, Y. H.; Lee, Y. M.; Lee, J. Y.; Ko, M. J.; Yoo, P. J. Hierarchical Nanoflake Surface Driven by Spontaneous Wrinkling of Polyelectrolyte/Metal Complexed Films. *ACS Nano* **2012**, *6* (2), 1082-1093.
- (43) Kim, J. B.; Kim, P.; Pégard, N. C.; Oh, S. J.; Kagan, C. R.; Fleischer, J. W.; Stone, H. A.; Loo, Y.-L. Wrinkles and deep folds as photonic structures in photovoltaics. *Nat. Photonics* **2012**, *6* (5), 327-332. DOI: 10.1038/nphoton.2012.70.
- (44) Li, M.; Hakimi, N.; Perez, R.; Waldman, S.; Kozinski, J. A.; Hwang, D. K. Microarchitecture for a three-dimensional wrinkled surface platform. *Adv. Mater.* **2015**, *27* (11), 1880-1886. DOI: 10.1002/adma.201405851.
- (45) Xie, J.; Han, X.; Ji, H.; Wang, J.; Zhao, J.; Lu, C. Self-Supported Crack-Free Conducting Polymer Films with Stabilized Wrinkling Patterns and Their Applications. *Sci. Rep.* **2016**, *6*, 36686. DOI: 10.1038/srep36686.
- (46) Rogers, J. A.; Someya, T.; Huang, Y. J. S. Materials and Mechanics for Stretchable Electronics. *Science* **2010**, *327* (5973), 1603-1607. DOI: 10.1126/science.1182383
- (47) Xu, S.; Yan, Z.; Jang, K. I.; Huang, W.; Fu, H.; Kim, J., ... & Rogers, J. A. . Assembly of micro/nanomaterials into complex, three-dimensional architectures by compressive buckling. *Science* **2015**, *347* (6218), 154-159.

- (48) Li, Y.; Tian, X.; Gao, S. P.; Jing, L.; Li, K.; Yang, H.; Fu, F.; Lee, J. Y.; Guo, Y. X.; Ho, J. S.; Chen, P. Y.. Reversible Crumpling of 2D Titanium Carbide (MXene) Nanocoatings for Stretchable Electromagnetic Shielding and Wearable Wireless Communication. *Adv. Funct. Mater.* **2019**, *30* (5), 1907451. DOI: 10.1002/adfm.201907451.
- (49) Wang, Y.; Li, J.; Xie, Y.; Hu, J.; Zhu, X.; Sun, S.; Jing, X.; Mi, H. Y.; Liu, C.; Shen, C. Fabrication of wrinkled thermoplastic polyurethane foams by dynamic supercritical carbon dioxide foaming. *J. Supercrit. Fluids* **2022**, *180*, 105429. DOI: 10.1016/j.supflu.2021.105429.
- (50) Jun, L.; Qin, Z.; Mi, H. Y.; Dong, B. B.; Liua, C.; Shena, C. Fabrication of Thermoplastic Polyurethane Foams with Wrinkled Pores and Superior Energy Absorption Properties by CO₂ Foaming and Fast Chilling. *Macromol. Mater. Eng.* **2022**, *307* (1), 2100600. DOI: 10.1002/mame.202100600.
- (51) Li, B.; Jia, F.; Cao, Y. P.; Feng, X. Q.; Gao, H. Surface wrinkling patterns on a core-shell soft sphere. *Phys. Rev. Lett.* **2011**, *106* (23), 234301. DOI: 10.1103/PhysRevLett.106.234301.
- (52) Brojan, M.; Terwagne, D.; Lagrange, R.; Reis, P. M. Wrinkling crystallography on spherical surfaces. *Proc. Natl. Acad. Sci. U. S. A.* **2015**, *112* (1), 14-19. DOI: 10.1073/pnas.1411559112.
- (53) Stoop, N.; Lagrange, R.; Terwagne, D.; Reis, P. M.; Dunkel, J. Curvature-induced symmetry breaking determines elastic surface patterns. *Nat. Mater.* **2015**, *14* (3), 337-342. DOI: 10.1038/nmat4202.
- (54) Yang, S.; Khare, K.; Lin, P. C. Harnessing Surface Wrinkle Patterns in Soft Matter. *Adv. Funct. Mater.* **2010**, *20* (16), 2550-2564. DOI: 10.1002/adfm.201000034.

- (55) Xu, Z. M.; Jiang, X. L.; Liu, T.; Hu, G. H.; Zhao, L.; Zhu, Z. N.; Yuan, W. K. Foaming of polypropylene with supercritical carbon dioxide. *J. Supercrit. Fluids* **2007**, *41* (2), 299-310. DOI: 10.1016/j.supflu.2006.09.007.
- (56) Hu, D.; Zhou, C.; Liu, T.; Chen, Y.; Liu, Z.; Zhao, L. Experimental and numerical study of the polyurethane foaming process using high-pressure CO₂. *J. Cell. Plast.* **2021**, *57* (6), 927-949 DOI: 10.1177/0021955x20974291.
- (57) Bates, S. R. G.; Farrow, I. R.; Trask, R. S. Compressive behaviour of 3D printed thermoplastic polyurethane honeycombs with graded densities. *Mater. Des.* **2019**, *162*, 130-142. DOI: 10.1016/j.matdes.2018.11.019.
- (58) Wang, X. C.; Zhu, Q. S.; Dong, B. B.; Wu, H.-H.; Liu, C. T.; Shen, C. Y.; Turng, L. S.; Geng, T. The effects of nanoclay and deformation conditions on the inelastic behavior of thermoplastic polyurethane foams. *Polym. Test.* **2019**, *79*, 106043. DOI: 10.1016/j.polymertesting.2019.106043.

Table of Content

